Excitation of Single-Mode Shear-Horizontal Guided Waves and Evaluation of Their Sensitivity to Very Shallow Crack-Like Defects

Pouyan Khalili and Frederic Cegla, *Member, IEEE*

***Abstract*— Inspection is a key part of the asset management process of industrial plants and there are numerous plate-like structures that require inspection. Ultrasonic guided waves have been extensively used to detect various types of defect by monitoring reflected and transmitted signals because they enable faster screening of large areas. However, ultrasonic guided wave testing becomes difficult for very shallow, sharp defects as current inspection techniques suffer from a lack of sensitivity to such features. Previous studies, obtained by comparing various inspection techniques, suggest that the SH1 mode in particular, at around 3 MHz · mm, would be suitable when testing for shallow defects; however, it is clear that both the SH0 and SH1 modes can exist at this frequency–thickness product. This can complicate the inspection process and, therefore, limit defect detectability. This article investigates the possibility of a single-mode excitation of the SH1 mode at around 3 MHz · mm. The ability of this method toward detecting very shallow defects (<10% cross-sectional thickness loss) has also been studied. By means of analytical predictions and finite element, it is shown that a signal dominated by the SH1 mode can be generated using a single permanent periodic magnet (PPM) electromagnetic acoustic transducer (EMAT) (PPM EMAT). All predictions are then backed up by experimental measurements. It is also shown that, by studying the reflection coefficient of the SH1 mode, the pure SH1 mode can be used to detect defects as shallow as 5% thickness loss from a 500-mm standoff. These defects would otherwise be missed by standard, lower frequency guided wave testing.**

***Index Terms*— 2-D fast Fourier transform (FFT), defect sensitivity, mode-selectivity, permanent periodic magnet (PPM) electromagnetic acoustic transducers (EMAT), shear-horizontal (SH) guided wave.**

I. Introduction

INSPECTION is a key part of the asset management process [1] and there are numerous plate-like structures that require inspection. Ultrasonic guided waves have been extensively used to detect various types of defect by monitoring reflected and transmitted signals [2]–[5]; however, testing becomes difficult for sharp, shallow defects (<10% cross-sectional thickness loss) as current inspection techniques suffer from a lack of sensitivity to such features.

A number of studies point toward the use of shear horizontal (SH) guided waves [6]–[10] when inspecting for defects such as cracks and corrosion patches. Furthermore, SH waves are also becoming more popular for applications such as pipeline tomography [11], [12]. SH guided waves provide an alternative inspection method to Lamb waves since they exhibit simpler dispersion characteristics and are unaffected by nonviscous liquid loading. There are various industrial application examples [13], [14] which employ electromagnetic acoustic transducers (EMATs) in an automatic inspection system to scan for defects in the axial and circumferential directions; a transmission configuration is used for the circumferential scan which can use the excitation transducer to receive waves that have traveled around the pipe circumference, while reflection in a pulse-echo configuration is measured for axial scans. There are also other examples of using higher order SH waves for structural corrosion monitoring [9]; such studies primarily consider the cutoff phenomenon of the higher order modes in order to estimate the minimum remnant thickness. In some cases [6], [7], the wavenumber changes in the thinning region and the consequent zero wavenumber value at cutoff thickness cause a total reflection of higher order SH modes; this is helpful for the detection of gradual surface corrosion.

The sensitivity of a method/guided wave mode toward a particular defect depends on various parameters such as its mode shape and dispersion characteristics, which are both frequency and thickness dependent. The SH guided wave dispersion curves are shown in Fig. 1; here, the presence of multiple wave modes at different frequency–thickness regimes is evident. Previous studies [15], [16], obtained by comparing various inspection techniques, suggest that the SH1 mode in particular, at around 3 MHz · mm, would be suitable when testing for shallow defects (testing at lower frequency–thickness values was found to be undesirable due to the excessive dispersion of the SH1 mode and the risk of operating close to its cutoff frequency); this is due to its high surface energy content and the dispersive nature of this mode which makes it sensitive

Manuscript received June 23, 2020; accepted July 16, 2020. Date of publication July 22, 2020; date of current version February 24, 2021. This work was supported by the Offshore Robotics for Certification of Assets (ORCA) Hub through the Engineering and Physical Sciences Research Council (EPSRC) under Grant EP/R026173/1. *(Corresponding author: Pouyan Khalili.)*

The authors are with the Non-Destructive Evaluation Group, Mechanical Engineering Department, Imperial College London, London SW7 2AZ, U.K. (e-mail: p.khalili14@imperial.ac.uk; f.cegla@imperial.ac.uk).

Digital Object Identifier 10.1109/TUFFC.2020.3011226

This work is licensed under a Creative Commons Attribution 4.0 License. For more information, see https://creativecommons.org/licenses/by/4.0/

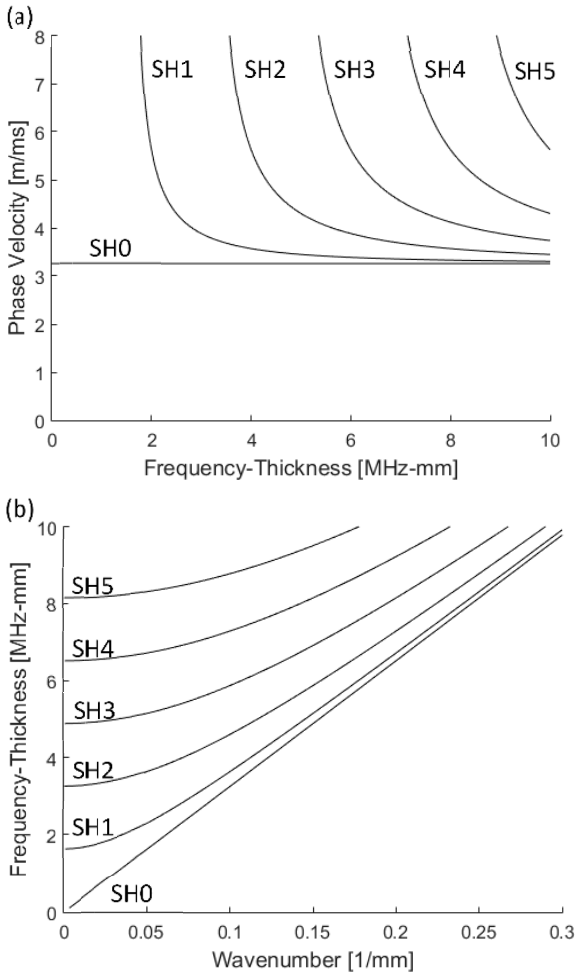


Fig. 1. SH wave dispersion curves in a steel plate showing (a) phase velocity and (b) wavenumber generated using DISPERSE software [19].

to cross-sectional thickness changes. However, it is clear from Fig. 1 that both the SH0 and SH1 modes can exist at the desired 3 MHz · mm frequency–thickness product. This can complicate the inspection process since multiple echoes are recorded in a time trace and therefore, the defect detectability can be complicated and limited. Hence, selective SH1 mode excitation is very desirable to build simple inspection systems. There have been a number of studies [17], [18] which investigate the possibility of pure SH1 mode excitation by using dual permanent periodic magnet (PPM) EMATs placed on either side of the waveguide; this, clearly, requires access to both surfaces of the structure which is unfeasible when inspecting components such as pipes and storage tanks where there is limited access to the inner surfaces.

This article investigates the possibility of a single-mode excitation of the SH1 mode at around 3 MHz · mm using a single-PPM EMAT. The ability of this method toward detecting very shallow defects (<10% cross-sectional thickness loss) has also been studied.

Section II gives a brief background on the physics of EMATs used to excite the SH guided modes and outlines the design parameters which determine the ability of such transducers to generate a pure mode; this section also highlights the practical advantages of EMATs when compared to piezoelectric (PZT) probes. Section III then introduces the analytical prediction of the excitation force bandwidths for a given EMAT setup through the use of a Fourier transform in time and space [2-D fast Fourier transform (FFT)]. Then these predictions are verified via finite-element (FE) analysis in Section IV, where the sensitivity of the SH1 mode toward very shallow defects is also investigated. Finally, the analytical and numerical predictions are verified experimentally in Section V and the findings are summarized in Section VI.

II. Background

SH guided waves, similar to all shear waves, exhibit a displacement field perpendicular to its propagation direction; this, in a plate-like waveguide, means an in-plane displacement field while the wave packet propagates parallel to the waveguide boundaries. It has been previously shown [20], [21] that such waves can be generated by PZT probes where the oscillation of the piezoelectric element generates an ultrasonic wave which is transmitted via an angled Perspex wedge and ultrasonic coupling gel onto the metal waveguide surface. This provides strong signal amplitudes and can be implemented with basic NDE equipment but requires direct surface contact. Inconsistent coupling over the footprint, particularly over curved or rough surfaces, is a problem; there are also issues with poor high-temperature performance and reverberations within the wedge.

EMATs on the other hand rely on the interaction of the eddy currents generated by a coil and the bias magnetic field of a permanent (or electro) magnet to produce a force resulting in generation of elastic waves in the structure [22], [23]. Hence, they do not require direct contact which eliminates the need for a couplant; this allows transduction through thin coatings/paint and rough surfaces and also results in good high temperature performance; however, they suffer from poor signal-to-noise ratio (SNR) and often require bulky and heavy electronics.

In the case of SH guided waves, periodic permanent magnet array (PPM) EMATs can be used for generation and detection. PPM EMATs consist of an array of permanent magnets which is located above a race-track coil. The coil can be made in a form of a printed circuit board (PCB) [8], [10]. Fig. 2 shows a typical PPM EMAT configuration. The performance of such a transducer is determined by its frequency and wavenumber bandwidths. Here, the frequency bandwidth is determined by the nature of the excitation signal in time; typically, for guided wave applications, this is specified by the center frequency, the number of cycles used, and the window applied [24]. The polarization and the spacing between the magnets determine the nature of the Lorentz force induced on the waveguide surface which in turn dictates the wavelength (λ) and, hence, the wavenumber bandwidth of the probe. It is noteworthy that due to the unique design of PPM EMATs, compared to meander coil EMATs [25], the excitation wavelength is dictated by the magnet arrangement/size rather than the coil which means the performance of this type of transducer is limited to the strength of the field generated by the magnets. This can be problematic when using PPM EMATs for higher frequency wave excitation (due to small wavelength, the magnet array must be shrunk which results in lower energy transmission).

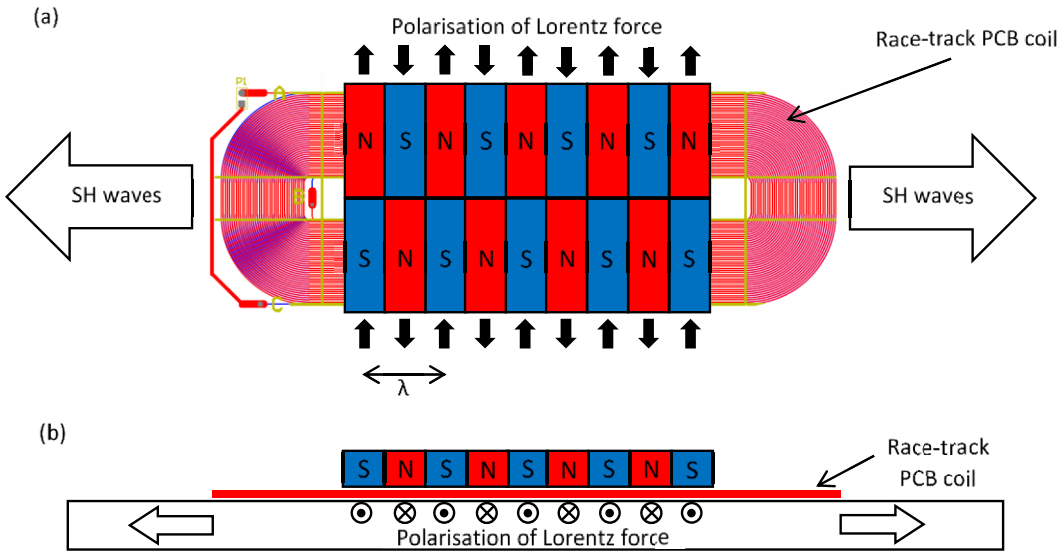


Fig. 2. Schematic of (a) PPM EMAT showing coil, magnet array, and the direction of the resulting Lorentz force as well as the propagation direction of the SH waves (top view) and (b) coil and magnet array on plate cross section (side view).

Evidently, there are a number of design parameters which determine the ability of a PPM EMAT toward pure mode excitation; in order to establish the possibility of a single-mode excitation of the SH1 mode at around 3 MHz · mm using such probes, an analytical model was developed which allows the prediction of the excitation force bandwidths for a given setup through the use of a 2-D FFT. There have been previous studies [26] which describe the use of 2-D FFT in detail.

III. Analytical Predictions of the Excitation Force Bandwidths

The response amplitude of a mode in a waveguide at a particular frequency and wavenumber is directly related to the excitation force acting on the surface at the corresponding frequency and wavenumber [24]. As mentioned above, the frequency and wavenumber bandwidths are dictated by the nature of the transducer design, so it is necessary to investigate how to obtain the optimal setup for pure SH1 mode excitation in the desired frequency–thickness product. Here, a simple 2-D analytical model, implemented in the MATLAB software, was employed as it can capture the essential physics while enabling the rapid study of a large number of probe configurations [24], [25]. In order to predict the wavenumber and frequency bandwidths of the excitation force, the surface force generated by the PPM EMAT was simulated by an array of in-plane surface point forces followed by the use of a Fourier transform in space and time (2-D FFT). Analytical calculations were carried out for a steel plate ($C_L = 5960$ m/s, $C_S = 3260$ m/s, $\rho = 7932$ kg/m^3) and the material was assumed to be isotropic. It is worthwhile noting that aluminum has very similar dispersion characteristics and it is, therefore, to be concluded that the same design criteria will work well for exciting SH1 waves in aluminum.

The force pattern for the PPM EMAT was determined by an array of in-plane surface forces with opposite polarity depending on the direction of the acting Lorentz force (as shown in Fig. 2); this pattern is repeated according to the wavelength (λ) and the number of cycles of the magnets in space. Here, for simplicity, the force acting on the surface was assumed to be constant across the width of the magnet [3]. The excitation signal was, therefore, determined by the applied signal in time and the polarity of the Lorentz force.

As stated above, the pure SH1 mode excitation at around 3 MHz · mm (300-kHz center frequency in a 10-mm steel plate) is of interest; the wavelength of the SH1 mode at this frequency–thickness value is around 13 mm which was calculated using the DISPERSE software [19]. Some examples of the effects of the number of wavelengths in space and the signal in time are shown in Fig. 3. The left-hand column shows the excitation force amplitude for various PPM EMAT setups, while their corresponding excitation force wavenumber bandwidths at a center frequency of 300 kHz are illustrated on the right-hand column. The influence of the number of wavelengths in space is shown in Fig. 3(a) and (b) where the reduction of wavenumber bandwidth, as the number of cycles in space is increased from 2 to 4 wavelengths, is apparent. This effect is clearly shown in Fig. 3(d) and (e) where the dashed lines represent the SH0 and SH1 wavenumbers (at 300-kHz center frequency). Fig. 3(c) illustrates the reduction of frequency bandwidth by increasing the excitation signal from 5 to 10 cycles. It is noteworthy that, as shown by Fig. 3(e) and (f), the wavenumber bandwidth remains unaffected upon changing the frequency bandwidth which demonstrates that, in the case of PPM EMATs, the wavenumber and frequency bandwidths are fully decoupled.

While setups, similar to the ones shown in Fig. 3(b) and (c), to maximize the force amplitude on the SH1 mode, the ratio of the force amplitude of the SH1 mode to that of other modes is often more important for mode purity than the absolute force amplitude [24]. In order to obtain the optimum setup toward pure SH1 mode excitation while minimizing the generation of the SH0 mode, different practical excitation setups were studied for PPM EMAT; for brevity, only

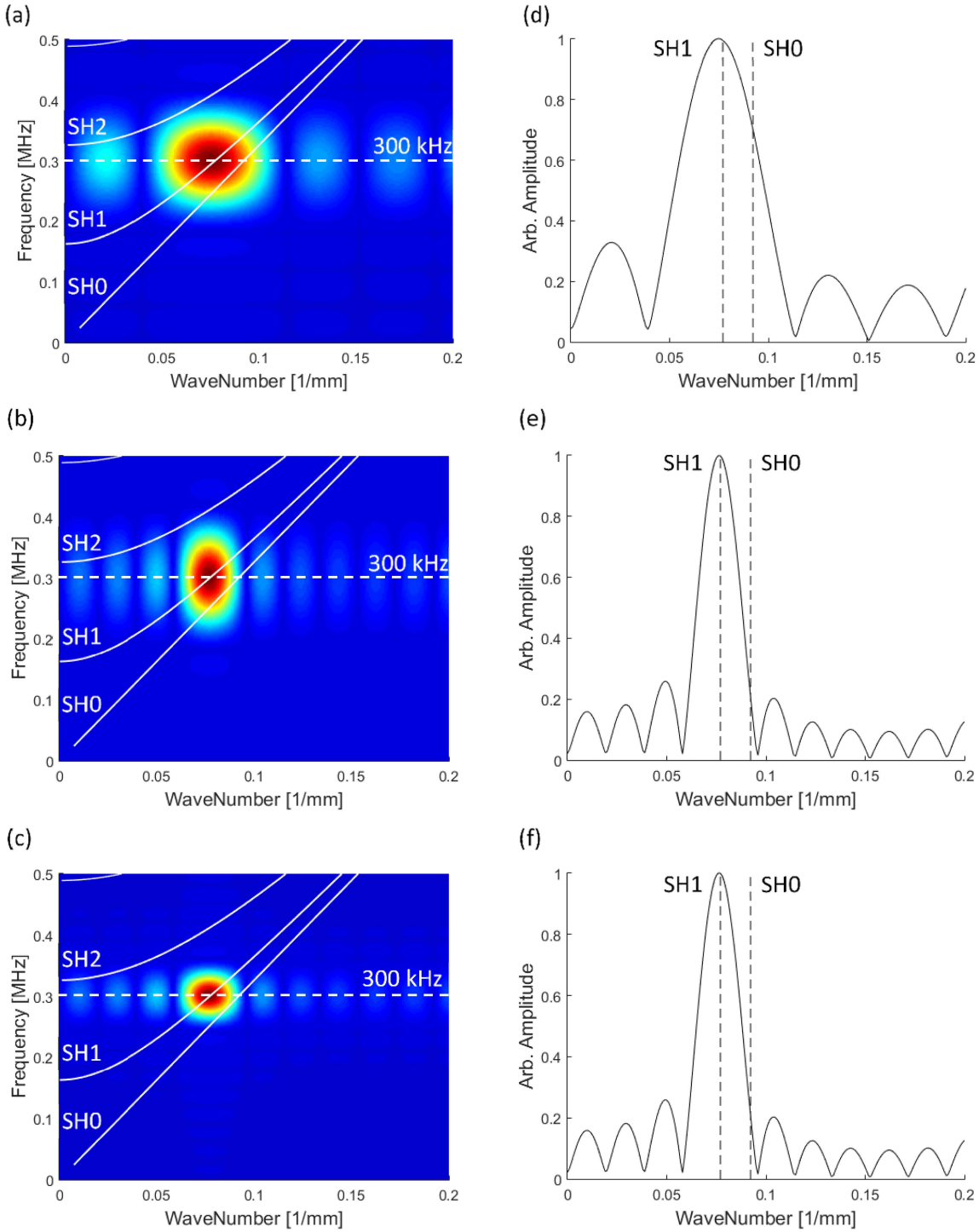


Fig. 3. Examples of 2-D FFT color plot [blue (low)–red (high) linear scale] for excitation configuration with wavelength in space, number of cycles in space, and number of cycles and window in time of (a) 13 mm, 2-cycle space, 5-cycle time Hanning; (b) 13 mm, 4-cycle space, 5-cycle time Hanning; and (c) 13 mm, 4-cycle space, 10-cycle time Hanning, respectively. Linear scale excitation amplitude as a function of wavenumber at the center frequency (300 kHz) obtained from (a) and (d); (b) and (e); and (c) and (f).

the optimized excitation configuration is presented in this article.

Fig. 4(a) shows the excitation force amplitude in frequency–wavenumber space for a 4-cycle PPM EMAT with a 14-mm wavelength in space (λ) and a 10-cycle Hanning-windowed toneburst signal in time at a center frequency of 300 kHz. It can be seen that due to the separation of the SH0 and SH1 dispersion curves, the use of a 4-cycle magnet setup in space and a 10-cycle toneburst signal in time provides sufficiently narrow wavenumber and frequency bandwidths for pure SH1 mode excitation. Also, as shown in Fig. 4(b), the sidelobes do not coincide with the undesired modes, hence maintaining pure mode excitation.

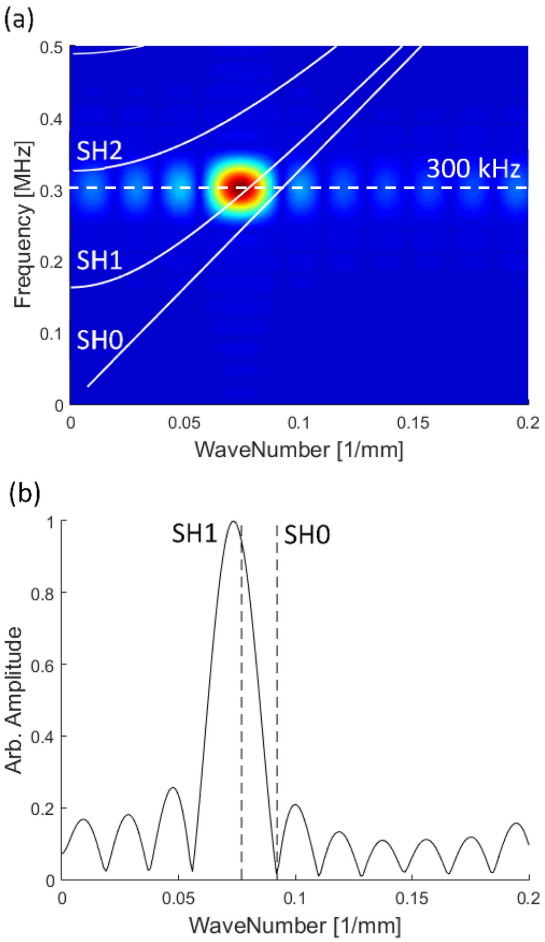


Fig. 4. (a) 2-D FFT color plot [blue (low)–red (high) linear scale] showing the excitation force amplitude in frequency–wavenumber space of a 4-cycle PPM EMAT with a 14-mm wavenumber in space and an excitation signal in time of a 10-cycle Hanning-windowed toneburst at a center frequency of 300 kHz and (b) force amplitude as a function of wavenumber at the center frequency (300 kHz) obtained from (a).

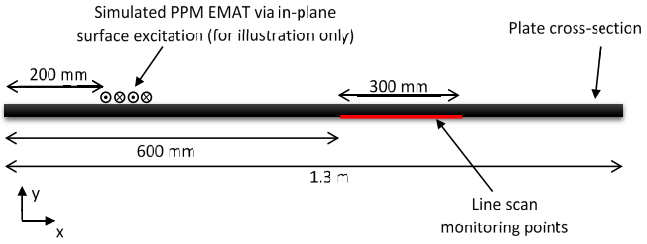


Fig. 5. Schematic of the general 2-D FE setup.

IV. Finite-Element Verification

FE was employed in order to verify the validity of the analytical predictions, where the excitation equivalent to that presented in Fig. 4 was applied and the in-plane surface displacement was output along a line; a 2-D FFT was performed to identify the modes excited within the waveguide. Additionally, a similar FE model was employed in order to establish the performance of the SH1 mode when used to inspect for very shallow cracks/defects with <10% cross-sectional thickness loss.

2-D models were considered in this study which allowed the investigation of the sound wave as it travels along the plate-like waveguide. The use of 2-D analysis means that the attenuation values reported do not include the effects of beam spreading, also the effects of diffraction around small defects are not captured; these effects will be investigated later via analytical means which allow the 2-D FE results to be extrapolated to obtain the realistic results which would have been highly

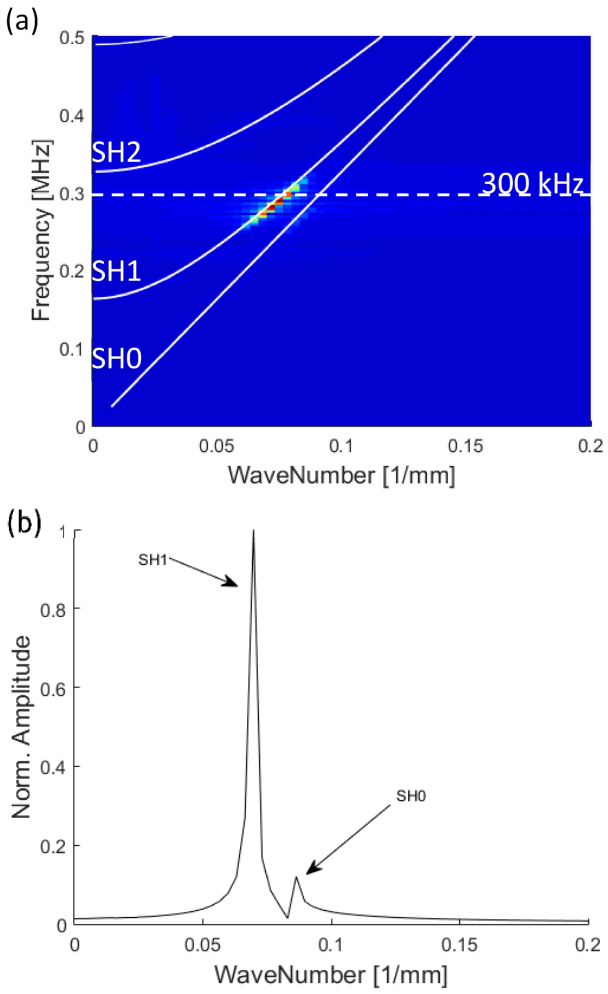


Fig. 6. (a) 2-D FFT color plot [blue (low)—red (high) linear scale] of the in-plane displacement recorded from 300-mm surface line scan for a simulated 4-cycle PPM EMAT with a 10-cycle Hanning tone burst in time at 300-kHz center frequency. (b) Amplitude as a function of wavenumber at the center frequency (300 kHz) obtained from (a).

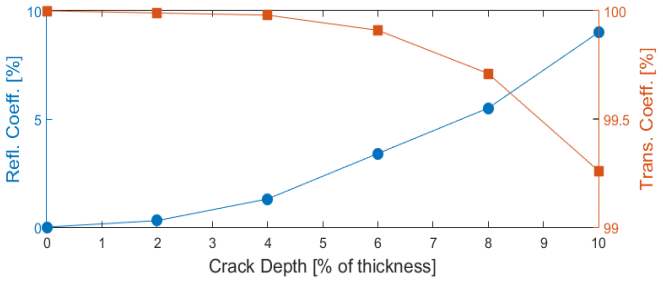


Fig. 7. 2-D FE predictions of the reflection and transmission coefficients (compared to the incident wave) of the SH1 mode at 300-kHz center frequency at the crack depths of 2%–10% in a 10-mm-thick plate. (Points are joined with straight lines to aid clarity.) (Different *y*-axis scales associated with the reflection and transmission coefficients on the respective left- and right-hand sides of the graph should be noted.)

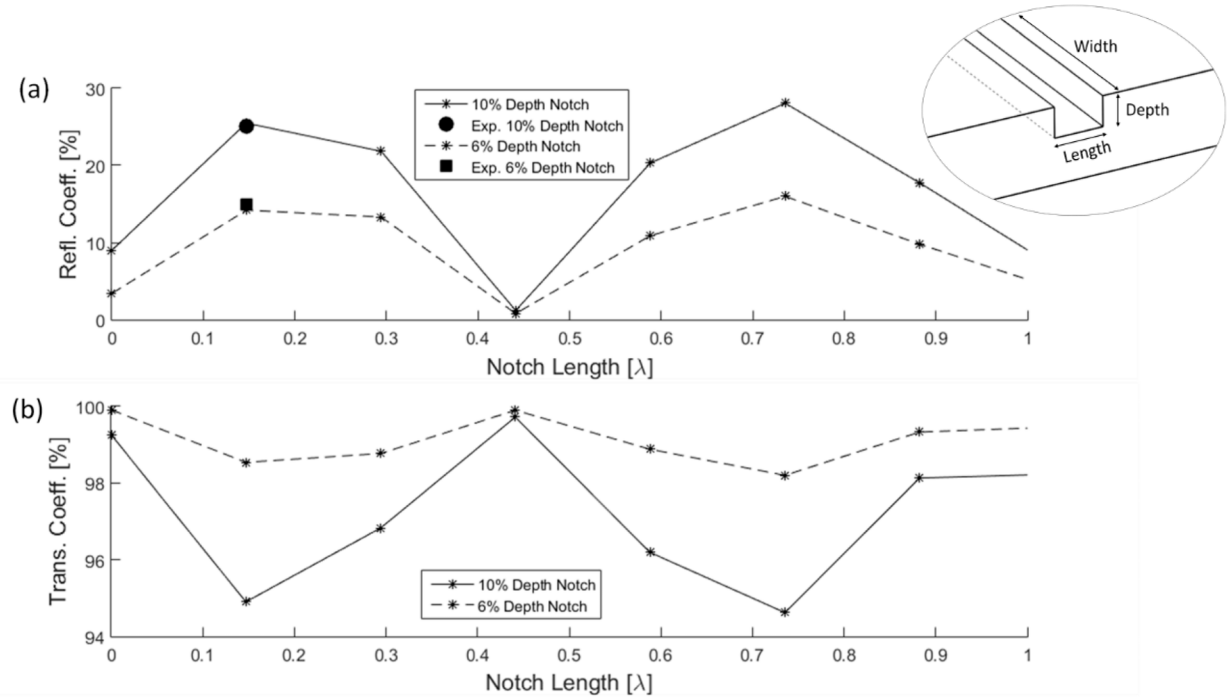


Fig. 8. 2-D FE predictions of the (a) reflection and (b) transmission coefficients (compared to the incident wave) of the SH1 mode at 300-kHz center frequency at a fixed defect depth of 10% and 6% with lengths of 0–λ in a 10-mm-thick plate. (Points are joined with straight lines to aid clarity.) (Schematic of the notch shows the dimension terminology that is used.) The experimental reflection ratios from the 10% and 6% thickness loss notches (obtained from Fig. 13) are also superimposed for comparison. (Different *y*-axis scales associated with the reflection and transmission coefficients should be noted.)

complex and computationally expensive to obtain from full 3-D models.

A. FE Model Setup

Fig. 5 shows the overall FE setup, where a 10-mm-thick steel plate was created using CPE4R elements (linear elastic material properties were considered) in the ABAQUS CAE commercial software; 0.1-mm cubic elements and a 40-ns time step were applied according to the operational frequency that was used in each simulation so that stability and accuracy were maintained. Excitation with a 4-cycle PPM EMAT with a 14-mm wavelength was simulated by in-plane surface point forces, while the excitation in time was a 10-cycle Hanning-windowed toneburst at a center frequency of 300 kHz. A 300-mm surface line scan was employed to perform the 2-D FFT that was used to identify the induced SH modes in the plate.

A similar FE setup to the one shown in Fig. 5 was used to investigate the sensitivity of the SH1 mode to very shallow crack-like defects. In order to record the reflected and transmitted waves, 300-mm surface line scan monitoring points were employed before and after the defective region, respectively. In this article, zero-volume cracks, with depths ranging from 2% to 10%, were considered; these were simulated by disconnected nodes in the FE mesh. Additionally, notches with lengths ranging from 0 (crack) to 1λ (wavelength of the SH1 mode at 3 MHz $\cdot$ mm) were also studied.

B. Modal Decomposition Using 2-D FFT

The 2-D FFT was performed on the in-plane displacement time traces obtained from the 300-mm line scan surface monitoring points located around 300 mm from the excitation region. Fig. 6 shows the 2-D FFT linear scale color plot where the presence of a dominant SH1 mode is evident, while the SH0 mode exhibits lower amplitude. It is noteworthy that in an experimental setup, probes of the same design were used for excitation and reception, meaning that the SH0 mode would be further suppressed relative to the SH1 mode (due to reciprocity causing the further suppression of other modes) in practical testing.

C. Interaction of the Pure SH1 Mode With Shallow Crack-Like Defects

The interaction of the SH1 mode at around 3 MHz $\cdot$ mm with very shallow sharp, crack-like defects with depths ranging from 2% to 10% of the cross-sectional thickness of the waveguide was studied. Here, the sensitivity of this method to the depth of defect was established by predicting the reflection and transmission coefficients when interacting with a zero-volume crack; these were modeled by disconnecting nodes in the FE mesh. In this case, the reflection coefficient of the SH1 mode was calculated by isolating the reflected signal via baseline subtraction (obtained from an undamaged plate model) followed by the use of a 2-D FFT for modal decomposition purposes; the transmission coefficient was obtained via a 2-D FFT performed on the displacement time traces recorded by the line scan positioned after the defect.

Fig. 7 illustrates the predicted reflection and transmission coefficients of the SH1 mode as a function of the crack depth. It can be seen that the SH1 mode shows sensitivity in reflection to defects as small as 4% depth below which the reflection coefficient becomes practically insignificant; this is

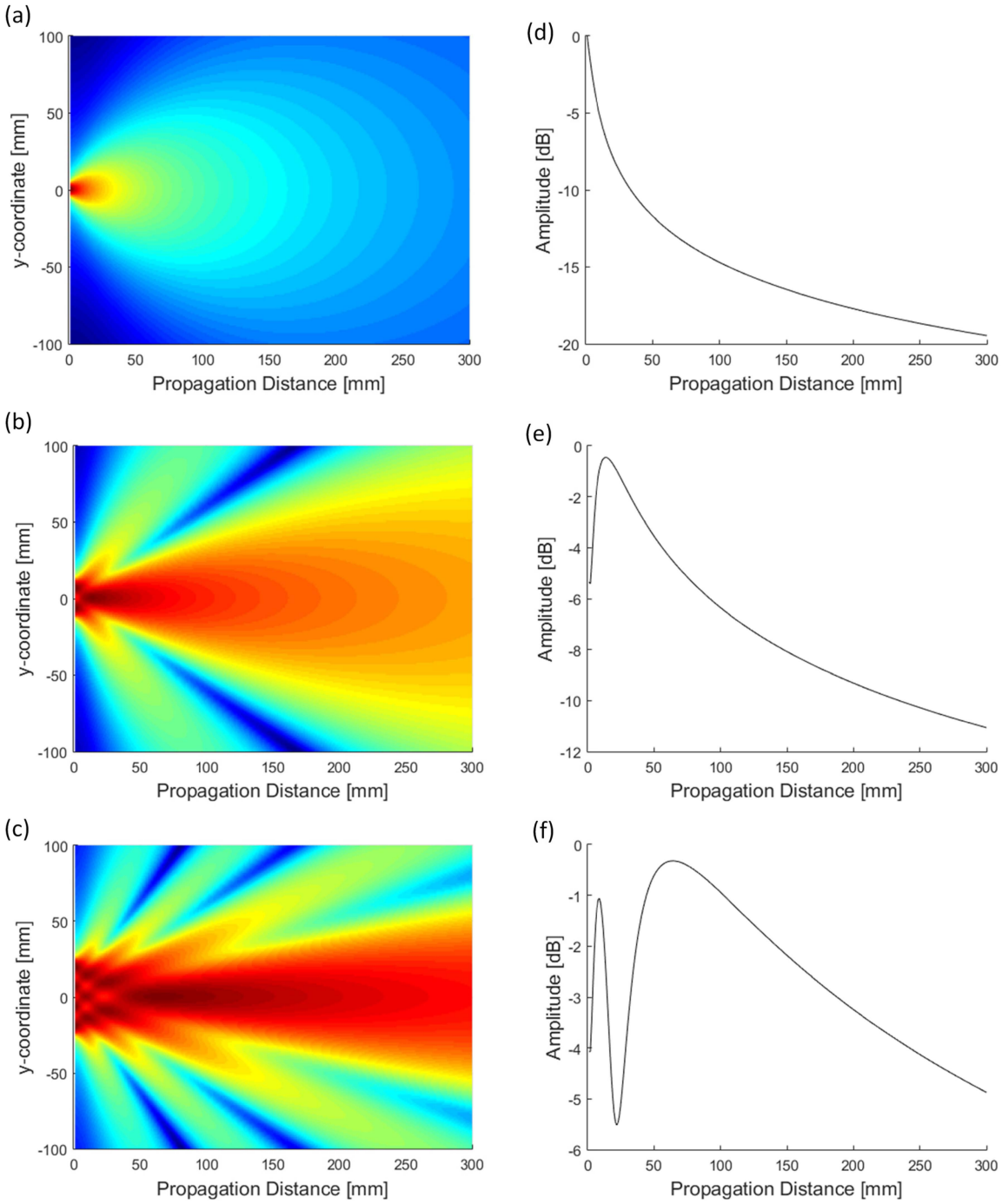


Fig. 9. Predicted color plot [blue (low)—red (high) logarithmic scale] of the reflection amplitude decay due to beam spread effect for defect apertures of (a) 10 mm; (b) 25 mm; and (c) 50 mm. Logarithmic scale center-line amplitude decay as a function of propagation distance obtained from (a) and (d); (b) and (e); and (c) and (f). The results were obtained for a wavelength of 13 mm, which correspond to those for the SH1 mode at 300-kHz center frequency on a 10-mm-thick plate, and it was assumed that each point of the defect is illuminated with the same amplitude.

firstly because of the mode shape of the SH1 mode which exhibits high surface energy, also this mode at 300 kHz in the 10-mm-thick plate is very dispersive and so is highly sensitive to the thickness of the structure. It is evident also that the SH1 mode experiences minimal mode conversion in transmission.

In order to investigate the effect of defect length on the performance of the SH1 mode, additional simulations were carried in order to predict the reflection and transmission coefficients of the SH1 mode when interacting with defects/notches with a fixed depth of 10% and 6% thickness loss and lengths ranging between 0 (crack) and 1λ.

Fig. 8(a) and (b) shows the reflection and transmission coefficients of the SH1 mode, respectively, obtained using a 2-D FFT, as a function of notch length for defect depths of 10% and 6%. The different scales for the reflection and transmission coefficients should be noted. Here, the interference effect as a function of defect length is clear; this is typically produced as the reflected wave from the step-down part of the defect interacts with the reflected wave from the step-up part of the

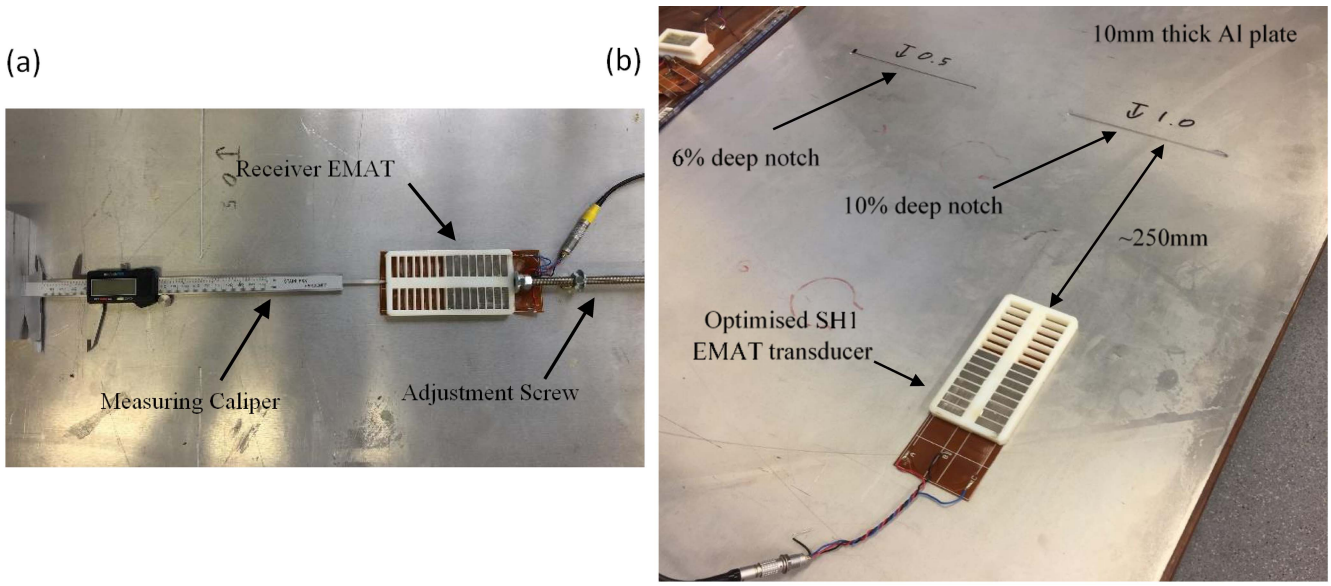


Fig. 10. Experimental setup on a 10-mm-thick aluminum plate used to (a) perform a 200-mm line scan for 2-D FFT purposes and (b) record pulse-echo measurements via a 4-cycle PPM EMAT at the center frequency of around 300 kHz. Setup (b) was employed to record the reflection from the 10% and 6% thickness loss notches as shown in the picture.

defect which depending on the length of the defect results in either constructive or destructive interference [27].

D. Effect of 3-D Beam Spread on Defect Detection

In order to investigate the practical sensitivity of the SH1 mode to realistic crack-like defects, the beam spread effect experienced by the reflected signal based on the aperture (width) of the defect was explored via a simple analytical model; here, the Huygens theory and the principle of superposition were employed to predict the amplitude decay of the reflected signal as a function of propagation distance and defect aperture in 3-D. Defect apertures of 50, 25, and 10 mm were considered. For each defect aperture, the reduction in the 2-D reflection coefficient (as shown in Figs. 7 and 8) was determined.

Fig. 9 shows the predicted amplitude decay for 10, 25, and 50 defect apertures as a function of the propagation distance; the respective center-line amplitude decays are displayed on the right-hand side. Here, the longer near field for larger apertures is evident, and additionally, it can be seen that the reflected signal experiences less beam spread as the defect aperture is widened; this is due to the aperture being multiple times the wavelength of the SH1 mode.

V. Experimental Validation

In order to establish the validity of the analytical and FE predictions of the possibility of pure SH1 mode excitation at around 3 MHz · mm values, experimental measurements on an aluminum plate were carried out. Initially, the nature of the incident beam was established via a pitch–catch measurement and a line scan followed by a 2-D FFT on an undamaged section of the waveguide/plate. In order to investigate the ability of the SH1 mode toward detecting very shallow defects, pulse-echo measurements were obtained on 200-mm-wide, 2-mm-long (equivalent to $\sim(1/7)\lambda$ of SH1 at 3 MHz · mm) notches with 10% and 6% thickness loss. Finally, to investigate the effect of defect aperture on the reflected signal, pulse-echo measurements were obtained as the EMAT probe was scanned across the width of the defect.

A. Experimental Setup

Fig. 10 illustrates the configuration of the experimental setup used to obtain the desired time traces on a 10-mm-thick aluminum plate. Excitation was performed at 3 MHz · mm (300-kHz center frequency) via a 10-cycle Hanning-windowed toneburst with a 4-cycle PPM EMAT with a 14-mm wavelength in space. The toneburst was generated by a computer-controlled HandyScope HS5 (TiePie Engineering Ltd., Town, The Netherlands) with an arbitrary wave generator (AWG) and oscilloscopes; the excitation signal was then amplified via a custom-built low power amplifier and fed into the transducer in order to generate the outgoing incident wave. The recorded signals from the transducer were then amplified by ~70 dB and fed back into the HS5, for sampling. In order to achieve the desired SNR value, all the measurements were carried out with 50 averages.

B. Pure SH1 Mode Excitation Results

Fig. 11 shows the time trace obtained in pitch–catch configuration using a similar PPM EMAT (not shown in Fig. 10) as used for excitation over propagation distances of around (a) 300 mm and (b) 500 mm. Here, the group velocity of the wave packet was obtained through time-of-flight measurements where the peak of the wave packet was obtained from a Hilbert transform of the time trace. The wave packet shown in Fig. 11 had a group velocity of 2640 m/s, which is within 1% of the group velocity of the SH1 mode obtained from the DISPERSE software [19]. The arrival time of the SH0 mode is also displayed in Fig. 11; here, it is clear that the presence of the SH0 mode is negligible.

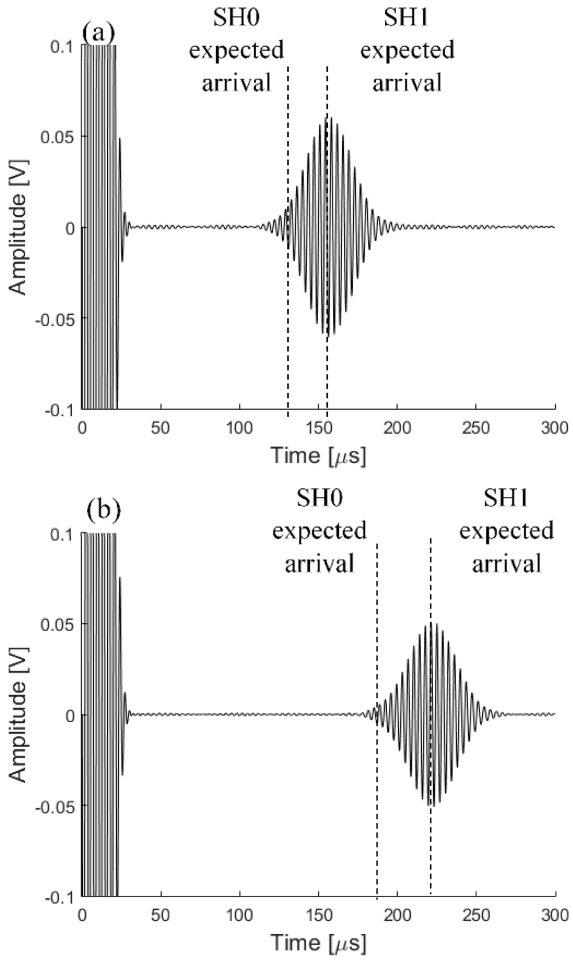


Fig. 11. Time trace obtained in pitch–catch configuration on a 10-mm aluminum plate with around (a) 300 mm and (b) 500 mm, and probe separation using two similar PPM EMATs consisting of a 4-cycle magnet array with 14-mm wavelength in space where the excitation was performed with a 10-cycle Hanning-windowed toneburst at 300-kHz center frequency. The expected [19] arrival times for the SH0 and SH1 modes are also indicated.

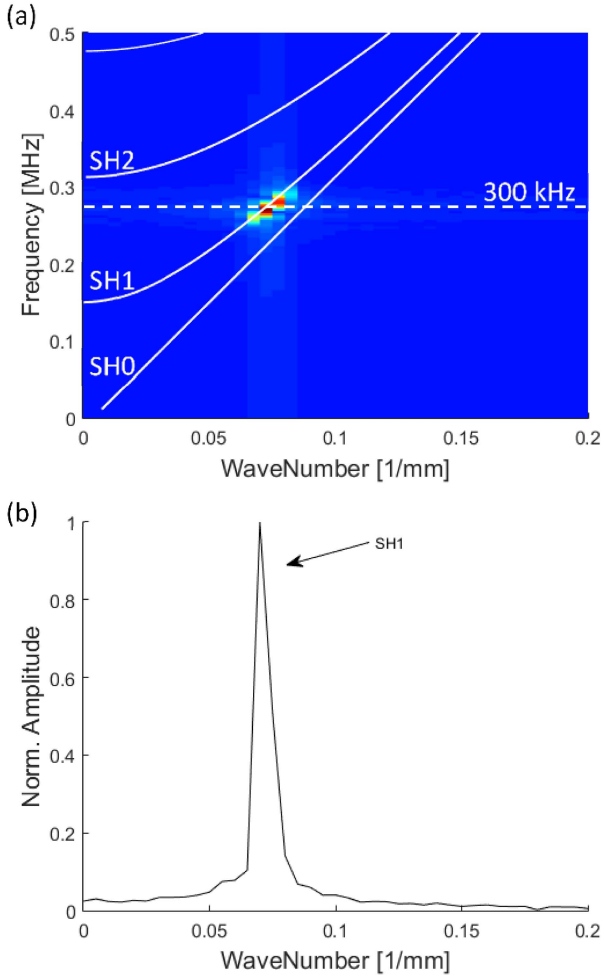


Fig. 12. (a) 2-D FFT color plot [blue (low)–red (high) linear scale] of experimental signal recorded surface line scan using two identical optimized PPM EMATs where the excitation was performed with a 10-cycle Hanning-windowed toneburst at 300-kHz center frequency and (b) amplitude as a function of wavenumber at the center frequency (300 kHz) obtained from (a).

To further confirm the purity of the SH1 mode, a 2-D FFT was performed on the time traces obtained in pitch–catch from a 200-mm line scan; as shown in Fig. 10(a), the receiver EMAT was moved at 1-mm intervals in the direction of propagation using a fine adjustment screw which was employed to push the probe along guiding tracks and to measure the movement of the probe, a digital Vernier caliper was used. Fig. 12(a) shows the amplitude in the frequency–wavenumber spectrum where the presence of the SH1 mode is clearly evident. Fig. 12(b) shows the amplitude as a function of wavenumber at the center frequency (300 kHz) obtained from the 2-D FFT of Fig. 12(a); here, the presence of the pure SH1 mode with negligible amplitude of the SH0 mode is clearly shown.

C. Defect Detection Results

Fig. 13 shows the pulse-echo time traces obtained around 250 mm behind the (a) 10% and (b) 6% thickness loss notches which were machined on the surface of the aluminum plate [as shown in Fig. 10(b)], where the sensitivity of the SH1 mode to very shallow defects is clearly evident. These measurements show 25% and 15% reflection ratios (compared to the incident wave amplitude) from the 10% and 6% thickness loss notches, respectively, which show good agreement to the predicted results [Fig. 8(a)]. It is also evident that the reflected wave packet contains both SH0 and SH1 due to mode conversion at the defect; however, because of the selectivity of the transducer in reception, the SH1 mode is shown to be the dominant mode in these time traces. Similar measurements were also carried out with the transducer placed around 500 mm behind the defect (the results are not shown in this article for brevity); here, a reflection ratio of 6% was obtained from the 6% thickness loss defect.

To further investigate the effect of defect aperture on the reflection ratio of the SH1 mode, pulse-echo measurements were obtained as the EMAT was scanned across the width (in the x-direction) of the defect in 5-mm intervals. The position of the EMAT is described as the relative offset between the bottom edge of the probe and the tip of the defect as shown in Fig. 14.

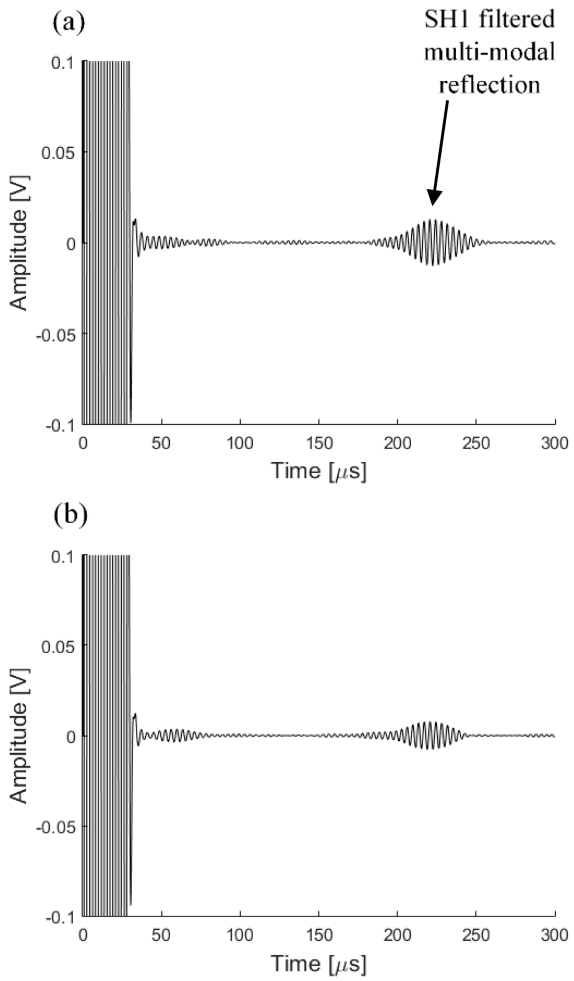


Fig. 13. Time traces obtained in pulse-echo configuration on a 10-mm aluminum plate around 250 mm behind a defect with (a) 10% thickness loss and (b) 6% thickness loss. Measurement was carried out with a PPM EMAT consisting of a 4-cycle magnet array with 14-mm wavelength in space where the excitation was performed with a 10-cycle Hanning-windowed toneburst at 300-kHz center frequency.

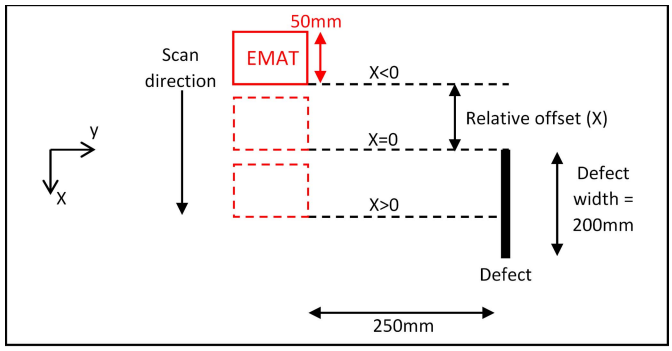


Fig. 14. Schematic of the experimental setup used to obtain pulse-echo measurements by scanning the optimized PPM EMAT across the width of the 10% thickness loss defect.

Fig. 15 shows the reflection ratio (compared to the incident wave) as a function of the relative offset between the bottom edge of the EMAT and the tip of the 10% thickness loss defect (as shown in Fig. 14). As expected, due to the negligible beam spread of the incident wave, no significant reflection is recorded when the defect is not geometrically in front of the EMAT. As the relative offset is increased, larger portion of the incident wave interacts with the defect which results in a larger reflection ratio as a result of the lower beam spread effect experienced by the reflected wave. The reflection ratio plateaus at ∼50-mm relative offset value since from this point forward, and the defect is fully covering the probe. It can be seen that at the relative offset of 25 mm (which is approximately equivalent to a 25-mm defect aperture), the reflection ratio is reduced by ∼9 dB compared to when the defect is fully covering the transducer (relative offsets >50 mm); this shows good agreement with the Huygens model [Fig. 9(b) and (e)] which predicted ∼10-dB reflection amplitude decay from a 25-mm aperture defect over a 250-mm propagation distance.

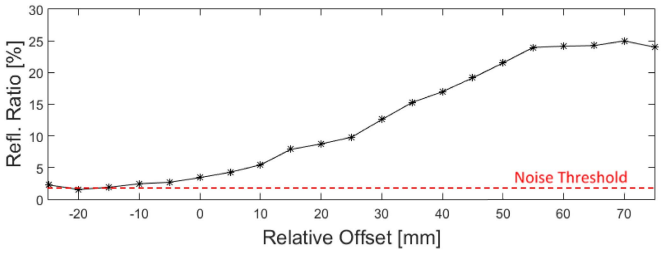


Fig. 15. Experimental reflection ratio (compared to the incident wave) as a function of the relative offset between the bottom edge of the optimized PPM EMAT probe and the tip of a 10% thickness loss notch. The signal noise level threshold is also shown. The measurement was obtained by scanning the probe across the width of the defect at 5-m intervals (points are joined with straight lines to aid clarity).

VI. Conclusion

The feasibility of pure SH1 mode excitation using a single-PPM EMAT at around 3 MHz · mm has been investigated. Excitation of the SH1 mode was considered due to the dispersive nature of this mode at around 3 MHz · mm and its mode shape which exhibits high surface energy; such properties are attractive for short/medium range inspection of very shallow crack-like defects.

Analytical predictions of the excitation force amplitude were obtained by simulating the surface Lorentz force associated with the PPM EMAT followed by the use of a 2-D FFT to highlight the excitation region in the wavenumber–frequency space. These were used to obtain the optimum excitation configuration for pure SH1 mode generation. It was predicted that a PPM EMAT consisting of a 4-cycle magnet array with a 14-mm wavelength in space enables selective excitation of the SH1 mode.

The optimum excitation setup was then applied to 2-D FE simulations. A 2-D FFT was performed on predicted in-plane surface displacements recorded in the form of a line scan. The results showed that a signal dominated by the SH1 mode could be generated. Similar FE simulations were carried out to predict the sensitivity of the SH1 mode to very shallow (<10% thickness loss) crack-like defects. In order to study the effect of defect depth on the propagation of the SH1 mode, the reflection and transmission coefficients of the SH1 mode

were recorded when interacting with zero-volume cracks with depths ranging from 2% to 10%. The influence of the defect lengths was also established by calculating the reflection and transmission coefficients from notches with fixed depth of 6% and 10% and lengths ranging from 0 to 1λ. Here, it was predicted that, zero-volume crack as shallow as 4% depth is likely to be detectable if excitation at an SNR value of above 40 dB is achievable, while, depending on the length of the notch, the reflection coefficients as high as 25% can be obtained from a 10% thickness loss notch.

Experimental measurements were carried out on a 10-mm-thick aluminum plate to validate the analytical and numerical predictions; modal decomposition was performed using a 2-D FFT on time traces obtained via a line scan with an optimized PPM EMAT. The measurements showed good agreement with the predicted results, establishing the possibility of pure SH1 mode excitation. Additionally, pulse-echo measurements were recorded around 250 mm behind 6% and 10% thickness loss defects. Here, reflection ratios of 15% and 25% were obtained, respectively, which showed good agreement with the simulated results, confirming the ability of this mode toward detecting very shallow crack-like defect.

REFERENCES

[1] (2020). *API Standards*. Accessed: Mar. 23, 2020. [Online]. Available: http://www.api.org

[2] R. Carandente, J. Ma, and P. Cawley, "The scattering of the fundamental torsional mode from axi-symmetric defects with varying depth profile in pipes," *J. Acoust. Soc. Amer.*, vol. 127, no. 6, pp. 3440–3448, Jun. 2010.

[3] B. Herdovics and F. Cegla, "Structural health monitoring using torsional guided wave electromagnetic acoustic transducers," *Struct. Health Monit., Int. J.*, vol. 17, no. 1, pp. 24–38, 2016.

[4] P. J. Mudge and P. Catton, "Quantification of defect size from long range guided wave ultrasonic tests on pipes," in *Proc. AIP Conf.*, 2008, vol. 975, no. 1, pp. 147–154.

[5] J. Ma and P. Cawley, "Low-frequency pulse echo reflection of the fundamental shear horizontal mode from part-thickness elliptical defects in plates," *J. Acoust. Soc. Amer.*, vol. 127, no. 6, pp. 3485–3493, 2010.

[6] Nurmalia, N. Nakamura, H. Ogi, M. Hirao, and K. Nakahata, "Mode conversion behavior of SH guided wave in a tapered plate," *NDT E Int.*, vol. 45, no. 1, pp. 156–161, Jan. 2012.

[7] N. Nakamura, H. Ogi, and M. Hirao, "Detection of shear horizontal guided waves propagating in aluminum plate with thinning region," *Jpn. J. Appl. Phys.*, vol. 50, no. 7S, Jul. 2011, Art. no. 07HC17.

[8] M. Hirao and H. Ogi, "An SH-wave EMAT technique for gas pipeline inspection," *NDT E Int.*, vol. 32, no. 3, pp. 127–132, Apr. 1999.

[9] P. Belanger, "High order shear horizontal modes for minimum remnant thickness," *Ultrasonics*, vol. 54, no. 4, pp. 1078–1087, Apr. 2014.

[10] A. C. Kubrusly, M. A. Freitas, J. P. von der Weid, and S. Dixon, "Interaction of SH guided waves with wall thinning," *NDT E Int.*, vol. 101, pp. 94–103, Jan. 2019.

[11] J. Wu, Z. Tang, K. Yang, S. Wu, and F. Lv, "Ultrasonic guided wave-based circumferential scanning of plates using a synthetic aperture focusing technique," *Appl. Sci.*, vol. 8, no. 8, pp. 1–18, 2018.

[12] D. K. Kim, J. K. Lee, H. M. Seung, C. I. Park, and Y. Y. Kim, "Omnidirectional shear horizontal wave based tomography for damage detection in a metallic plate with the compensation for the transfer functions of transducer," *Ultrasonics*, vol. 88, pp. 72–83, Aug. 2018.

[13] Sonomatic. (2020). *Topside SH-EMAT Inspection*. Accessed: Mar. 23, 2020. [Online]. Available: http://www.sonomatic.com

[14] Innerspec. (2020). *Temate MRUT (Medium Range UT)*. Accessed: Mar. 23, 2020. [Online]. Available: http://www.innerspec.com

[15] P. Khalili and P. Cawley, "The choice of ultrasonic inspection method for the detection of corrosion at inaccessible locations," *NDT E Int.*, vol. 99, pp. 80–92, Oct. 2018.

[16] R. Howard and F. Cegla, "On the probability of detecting wall thinning defects with dispersive circumferential guided waves," *NDT E Int.*, vol. 86, pp. 73–82, Mar. 2017.

[17] G. Qiu, X. Song, X. Zhang, J. Tu, and T. Chen, "Pure SH1 guided-wave generation method with dual periodic-permanent-magnet electromagnetic acoustic transducers for plates inspection," *Sensors*, vol. 19, no. 13, p. 3019, Jul. 2019.

[18] A. C. Kubrusly, M. A. Freitas, J. P. von der Weid, and S. Dixon, "Mode selectivity of SH guided waves by dual excitation and reception applied to mode conversion analysis," *IEEE Trans. Ultrason., Ferroelectr., Freq. Control*, vol. 65, no. 7, pp. 1239–1249, Jul. 2018.

[19] B. Pavlakovic, M. Lowe, D. N. Alleyne, and P. Cawley, "Disperse: A general purpose program for creating dispersion curves," *Rev. Prog. Quant. Nondestruct. Eval.*, vol. 16A, pp. 185–192, 1997.

[20] J. Li and J. L. Rose, "Excitation and propagation of non-axisymmetric guided waves in a hollow cylinder," *J. Acoust. Soc. Amer.*, vol. 109, no. 2, pp. 457–464, Feb. 2001.

[21] H.-J. Salzburger, F. Niese, and G. Dobmann, "EMAT pipe inspection with guided waves," *Weld. World*, vol. 56, nos. 5–6, pp. 35–43, May 2012.

[22] J. Isla, M. Seher, R. Challis, and F. Cegla, "Optimal impedance on transmission of Lorentz force EMATs," in *Proc. AIP Conf.*, vol. 1706, 2016, Art. no. 090012.

[23] R. Ribichini, F. Cegla, P. Nagy, and P. Cawley, "Study and comparison of different EMAT configurations for SH wave inspection," *IEEE Trans. Ultrason., Ferroelectr., Freq. Control*, vol. 58, no. 12, pp. 2571–2581, Dec. 2011.

[24] P. Khalili and P. Cawley, "Excitation of single-mode Lamb waves at high-frequency-thickness products," *IEEE Trans. Ultrason., Ferroelectr., Freq. Control*, vol. 63, no. 2, pp. 303–312, Feb. 2016.

[25] P. Khalili and P. Cawley, "Relative ability of wedge-coupled piezoelectric and meander coil EMAT probes to generate single-mode Lamb waves," *IEEE Trans. Ultrason., Ferroelectr., Freq. Control*, vol. 65, no. 4, pp. 648–656, Apr. 2018.

[26] D. Alleyne and P. Cawley, "A two-dimensional Fourier transform method for the measurement of propagating multimode signals," *J. Acoust. Soc. Amer.*, vol. 89, no. 3, pp. 1159–1168, Mar. 1991.

[27] A. Demma, P. Cawley, and M. Lowe, "Scattering of the fundamental shear horizontal mode from steps and notches in plates," *J. Acoust. Soc. Amer.*, vol. 113, no. 4, pp. 1880–1891, Apr. 2003.



Pouyan Khalili received the Ph.D. degree from Imperial College London, London, U.K., in 2018, with a focus on high-frequency guided waves and other methods of corrosion monitoring applied in petrochemical plants.

He has engaged with industrial partners such as EDF and Tenaris as a Technical Consultant working to provide novel inspection techniques for their specific applications. He is currently a Postdoctoral Research Associate with Non-Destructive Evaluation (NDE) Group, Mechanical Engineering Department, Imperial College London, specializing in low power of electronics for industrial NDT applications.



Frederic Cegla (Member, IEEE) is currently a Reader with Non-Destructive Evaluation (NDE) Group, Mechanical Engineering Department, Imperial College London, London, U.K.

He currently chairs the Physical Acoustics Group of the Institute of Physics of the U.K. and Ireland. He has been the holder of a prestigious EPSRC Fellowship and has won numerous awards such as the 2016 Achenbach medal for his contribution to the field of SHM over the last decade. He has an interest and track record in protecting and commercializing technology, the biggest success so far being the formation of Permasense Ltd., Crawley, U.K., a company that pioneered ultrasonic corrosion monitoring via autonomous wireless sensors. His research interests are in the fields of NDE, structural health monitoring (SHM), and physical acoustics.